IOP Publishing | Institute of Physics and Engineering in Medicine Physics in Medicine & Biology
Phys. Med. Biol. **00** (2016) 1–16 UNCORRECTED PROOF

Ex vivo detection of macrophages in atherosclerotic plaques using intravascular ultrasonic-photoacoustic imaging

AQ1

Nhat Quang Bui[1], Kyu Kyu Hlaing[1], Yong Wook Lee[2], Hyun Wook Kang[1,3] and Junghwan Oh[1,3]

[1] Interdisciplinary Program of Biomedical Mechanical & Electrical Engineering, Pukyong National University, Busan 48513, Korea
[2] School of Electrical Engineering, Pukyong National University, Busan 48513, Korea
[3] Department of Biomedical Engineering, Pukyong National University, Busan 48513, Korea

AQ2

E-mail: wkang@pukyong.ac.kr and jungoh@pknu.ac.kr

Received 18 July 2016, revised 12 November 2016
Accepted for publication 23 November 2016
Published

Abstract

Macrophages are excellent imaging targets for detecting atherosclerotic plaques as they are involved in all the developmental stages of atherosclerosis. However, no imaging technique is currently capable of visualizing macrophages inside blood vessel walls. The current study develops an intravascular ultrasonic-photoacoustic (IVUP) imaging system combined with indocyanine green (ICG) as a contrast agent to provide morphological and compositional information about the targeted samples. Both tissue-mimicking vessel phantoms and atherosclerotic plaque-mimicking porcine arterial tissues are used to demonstrate the feasibility of mapping macrophages labeled with ICG by endoscopically applying the proposed hybrid technique. A delay pulse triggering technique is able to sequentially acquire photoacoustic (PA) and ultrasound (US) signals from a single scan without using any external devices. The acquired PA and US signals are used to reconstruct 2D cross-sectional and 3D volumetric images of the entire tissue with the ICG-loaded macrophages injected. Due to high imaging contrast and sensitivity, the IVUP imaging vividly reveals structural information and detects the spatial distribution of the ICG-labeled macrophages inside the samples. ICG-assisted IVUP imaging can be a feasible imaging modality for the endoscopic detection of atherosclerotic plaques.

Keywords: atherosclerosis, indocyanine green, macrophages, photoacoustic imaging, ultrasound imaging

AQ3

(Some figures may appear in colour only in the online journal)

JNL:PMB PIPS: AA4F6B TYPE: PAP TS: NEWGEN DATE:10/12/16 EDITOR: IOP SPELLING: US

1. Introduction

Atherosclerosis is caused by a build-up of plaque in the inner lining of arteries and remains one of the leading causes of death worldwide despite state-of-the-art diagnostics and therapeutics (Hwang *et al* 2011). New diagnostic methods are still required to attain early detection of high-risk plaques, disease staging, and progression tracking. Recent research reveals that atherosclerotic plaque is induced by macrophages in white blood cells, which are originally sent by the immune system to clean up low-density lipoproteins cholesterol pockets as well as the fat accumulated in arteries (Van Gils *et al* 2012). The formation of atherosclerotic plaque is promoted by the persistence of fat-laden macrophages in the artery wall (Van Gils *et al* 2012). Therefore, macrophage cells can be excellent imaging targets to detect atherosclerotic plaque as the cells participate in all the stages of atherosclerosis including fatty streak formation, fibrous plaque progression, and, eventually, plaque rupture as well as thrombus formation (Libby *et al* 2009).

AQ4 Over the last decade, magnetic resonance imaging (MRI), with the use of ultrasmall superparamagnetic iron oxide nanoparticles as a contrast agent, has been widely employed in small animal and human studies for visualizing aorta and carotid plaques with accumulated macrophages (Schmitz *et al* 2001, Trivedi *et al* 2006, Tang *et al* 2009). MRI can archive relatively high resolution (10–100 μm at 3 T) and can provide the unique ability of combining functional, anatomical, and molecular information. In contrast, due to low sensitivity with the current contrast agent, MRI often requires a large amount of agents for diagnosis, and these agents are associated with toxicity (Hwang *et al* 2011). As a radioactive imaging modality with high sensitivity, positon emission tomography (PET) has been used to report plaque macrophage activity and to monitor anti-atherosclerosis therapy (Rudd *et al* 2002, Tahara *et al* 2006, Tawakol *et al* 2006). However, PET has a low spatial resolution (1–2 mm in micro-PET and 4–10 mm in clinical PET) due to intrinsic physical constraints. Optical imaging modalities such as near-infrared fluorescence and bioluminescence can provide the highest sensitivity and spatial resolution among the current imaging methods (Waldeck *et al* 2008, Yoo *et al* 2014). On the other hand, the modalities often suffer from a shallow penetration depth (~1 mm) due to strong light scattering in biological tissues, leading to limited clinical applicability. More recently, intravascular photoacoustic (IVPA) imaging has been reported to offer many advantages in the detection of atherosclerotic plaque (Wang *et al* 2010, 2014, Jansen *et al* 2013, Bai *et al* 2014). Due to high resolution and its sensitivity with relatively deep penetration, the modality could identify atherosclerosis; thus, multi-wavelength photoacoustic (PA) responses from the vessel wall could provide both structural and functional compositions of the plaque. Similar to PA imaging, IVPA imaging is a catheter-based imaging modality that relies on the PA effect (Vo-Dinh *et al* 2003, Wang 2009, De Montigny 2011). During IVPA imaging, acoustic signals normally result from transient thermal expansion due to the absorption of a nanosecond laser pulse in the sample. Then, an intravascular ultrasound (IVUS) transducer can be used to detect and collect acoustic waves to reconstruct IVPA images on the spatial distribution of light absorbers within the irradiated volume. Thus, IVPA imaging can effectively combine the sensitivity of optical imaging techniques with both the penetration depth and resolution of IVUS imaging (Sethuraman *et al* 2007, Wang *et al* 2010, Karpiouk *et al* 2012, Yang *et al* 2012, Bai *et al* 2014). In addition, the similarities between IVPA and IVUS imaging systems can allow a hybrid technique of the two imaging modalities, thus providing synthesis strengths such as the capability of visualizing and tracking interesting molecular imaging. Therefore, the IVUP imaging method may have a great potential for monitoring macrophages in atherosclerotic plaques.

Unfortunately, macrophages have insufficient optical absorption and, thus, can hardly be visualized using IVPA imaging. However, the optical absorption properties of the macrophages can be modified by labeling the cells with PA contrast agents. Indocyanine green AQ5 (ICG) as an intravenous tricarbocyanine dye with near-infrared absorbing properties has been approved by the US Food and Drug Administration (FDA) for assessing human cardiac output, liver blood flow and function, and retinal angiography (Fox *et al* 1957, Caesar *et al* 1961, Benson and Kues 1978, Flower 1995, Desmettre *et al* 2000). More importantly, ICG can detect certain molecular and cellular targets relevant to atherosclerosis (Yoneya *et al* 1998, Stanga *et al* 2003, Fischer *et al* 2006, Vinegoni *et al* 2011). For example, ICG can bind to low-density and high-density lipoproteins due to its lipophilic properties. Thus, the dye can enable *in vivo* detection of lipid-rich, inflamed atheroma, human atherosclerosis, and human macrophages (Yoneya *et al* 1998, Stanga *et al* 2003, Fischer *et al* 2006, Vinegoni *et al* 2011). After intravenous injection, ICG is rapidly bound to plasma proteins, taken up by the liver and then almost excreted, unchanged, into the bile. Typically, ICG has an elimination half-life of two to four min in subjects with normal liver function. However, once bound to proteins, ICG can be used as an intravascular angiographic agent for 40 min and eliminated from the bloodstream in two h. Thus, a short lifetime in blood circulation allows the repeated application of ICG. Moreover, ICG can be an excellent contrast agent for PA imaging with a maximum absorption at 785 nm in aqueous solution and at 805 nm in blood.

In this study, we explored the feasibility of identifying macrophages labeled with FDA-approved ICG to detect atherosclerotic plaques *ex vivo* by using a hybrid intravascular ultrasonic-photoacoustic (IVUP) imaging technique. Both tissue-mimicking vessel phantoms and atherosclerotic plaque-mimicking porcine arterial tissues were used to perform IVUS and IVPA imaging simultaneously. The acquired US and PA signals were quantified to evaluate the target structure as well as the spatial distribution of the ICG-labeled cells in terms of 2D cross-sectional images and signal amplitudes. 3D images of the cell-injected tissue were also reconstructed to identify the position of the ICG as well as the image contrast.

2. Materials and methods

2.1. IVUP imaging system

Figure 1(a) shows a digital photograph of a fabricated catheter used for IVUP imaging. Initially, a 600 μm core-diameter multimode optical fiber (MOF; BFL48-600, Thorlabs, NJ, USA) was used to irradiate each sample in a lateral direction. The fiber tip was polished at an angle of 38 degrees to entail the total internal reflection for side-firing. Then, the chamfered tip of the fiber was sealed with a customized glass cap for protection and refractive index mismatching by using two epoxy layers at both ends of the cap. Lastly, the side-firing fiber was integrated with a 45 MHz, single-element IVUS transducer (Revolution® 45 MHz catheter, Volcano, CA, USA) to fabricate the IVUP imaging catheter. It was confirmed that both the incident light and the IVUS transducer were co-aligned to irradiate and image the same AQ6 sample site. Thus, the fabricated IVUP catheter had a maximum outer diameter of 2.2 mm, and the length of the glass cap was 2.3 mm; as such the IVUP catheter is flexible and applicable for clinical interventional cardiology.

Figure 1(b) shows a schematic diagram of the experimental setups for *ex vivo* IVUP imaging based on a newly developed IVUP imaging system (Bui *et al* 2015). In brief, a tunable OPO laser (Surelite OPO Plus, Continuum, CA, USA) pumped by a Nd:YAG laser (Surelite III, Continuum, CA, USA) was employed as a light source. A 665 nm long-pass colored glass filter (FGL665S, Thorlabs, NJ, USA) was used to reject the pumping wavelength (532 nm),

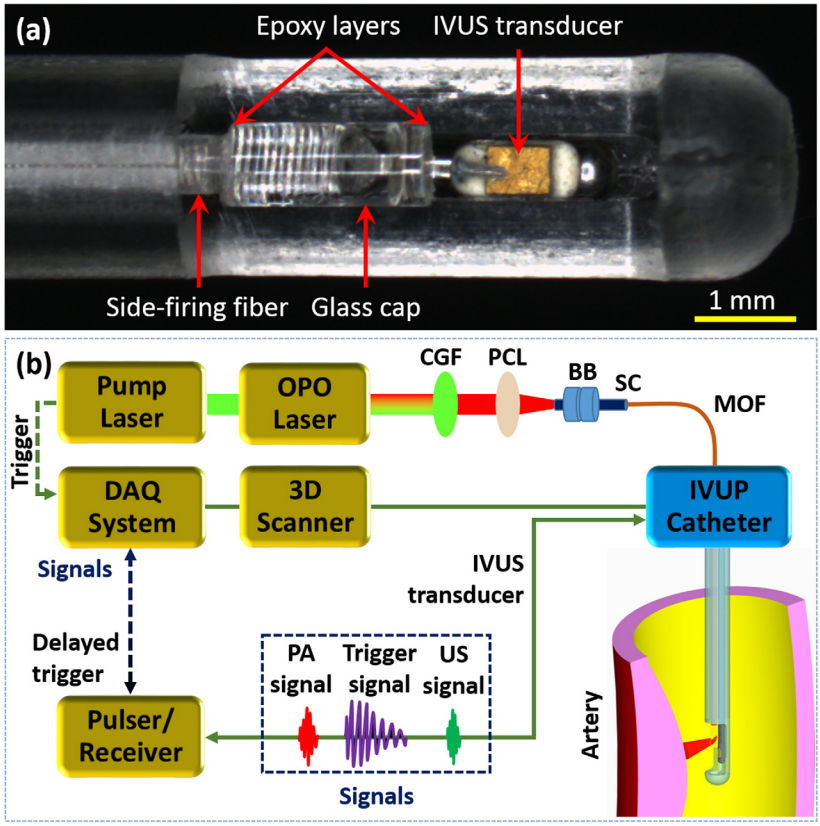

Figure 1. Illustration of IVUP imaging system: (a) microscopic image of distal end of IVUP catheter and (b) block diagram of experimental setups for *ex vivo* IVUP imaging (BB: ball bearing; CGF: colored glass filter; DAQ: data acquisition; IVUS: intravascular ultrasound; IVUP: intravascular ultrasonic-photoacoustic; MOF: multimode optical fiber; OPO: optical parametric oscillator; PA: photoacoustic; PCL: plano-convex lens; SC: SMA connector; US: ultrasound).

AQ7

and the filtered laser beam was coupled into a MOF using a plano-convex lens (LA1225-B, Thorlabs, NJ, USA). The input end of the MOF was fixed in a SMA905 multimode connector, which was rotatable using two ball bearings. The IVUP catheter was mounted on a 3D scanner to perform B-mode (cross-sectional images) scans along the circumference. A series of B-mode scans in a longitudinal direction was applied to reconstruct 3D images of each sample. An ultrasound pulse/receiver (USPR; 5900 PR, Olympus, MA, USA) was employed to generate electrical pulses to drive the IVUS transducer and to receive as well as to amplify both the laser-induced PA and US pulse-echo signals from the transducer. The detected PA and US signals are finally acquired by a data acquisition (DAQ; PXI-5124, National Instruments, TX, USA) system and converted into IVUP images via Hilbert transformation.

2.2. Signal sequence

Compared with the previous IVUP systems (Sethuraman *et al* 2007, Wang *et al* 2010, Karpiouk *et al* 2012, Yang *et al* 2012, Bai *et al* 2014), a delay pulse triggering technique was applied to the current system; as such it was able to sequentially acquire PA and US

signals from a single scan without using any external device. To avoid any signal overlapping between PA and US signals during IVUP imaging, the current study developed variable temporal sequences for signal acquisition by merely using a single DAQ system. Figure 2(a) shows a diagram of the signal sequences pre-determined in the DAQ system during the IVUP imaging. The total recording time of the digitizer was configured to be the sum of the lengths of the PA and the US signals. Due to the time of flight for a round-trip of each US wave, the recording time of the US signal was twice long as that of the PA signal. Thus, the total sampling length was three times as long as that of the PA signal. To simultaneously acquire both the PA and the US signals with a single scan, laser irradiation on the sample (i.e. start trigger from the laser source) immediately triggered the DAQ system to receive the PA signals generated from the sample. In addition, the light triggered the USPR to generate the US pulse signals after a constant delay from the onset of the irradiation. As the PA signals should be completely acquired prior to the generation of the US signals, the current study determined the delay time by using the PA signal length (i.e. reference position) was 37.5% longer than the physical distance between the transducer and sample. Figure 2(b) displays an example of both the PA (red) and US (blue) signals acquired from an 80 μm human black hair sample with a single A-line (1D time-resolved image) scan. As presented in figure 2(a), upon laser irradiation at 0 μs, the PA signal was generated and acquired from the sample 2.5 μs after the laser input; the distance between the transducer and the hair sample was 3.7 mm (i.e. 3.7 mm/1481 m s^{-1} = 2.5 μs). 4 μs (i.e. delay time) after the laser triggering, the USPR generated a triggering US signal with a signal length of 3 μs, and the echo US signal reflected from the sample was acquired 5 μs after the onset of the US triggering. It was noted that due to the round trip of the US signals (triggering and echo), the signal acquisition time of the US signal from the sample was twice as long as that of the PA signal (i.e. 2.5 μs for PA versus 5 μs for US).

2.3. Cell preparation

To assess the feasibility of identifying macrophages in atherosclerotic plaques, IVUP imaging was implemented on the ICG-loaded macrophage cells in phantoms and *ex vivo* arterial tissues. For cell preparation, macrophage cells (RAW 264.7, Korean Cell Line Bank, Seoul, South Korea) were grown in a Dulbecco's modified Eagle's medium (HyClone, UT, USA) mixed with 10% (by volume) fetal bovine serum (F6178 Sigma, Sigma-Aldrich, MO, USA) and a 1% antibiotic antimycotic solution (100×) (A5955 Sigma, Sigma-Aldrich, MO, USA) in 5% CO_2 at 37 °C. The media were changed every day, and the cells from the flask substrate were physically removed using a cell scraper. To prepare the ICG-loaded cells, the macrophage cells were washed twice with phosphate-buffered saline (PBS), added to a culture flask of 1 mg ml^{-1} of ICG solution in the media, and then incubated for one h in 5% CO_2 at 37 °C. The attached cells were then washed two more times with PBS and dislodged from the flask with a cell scraper. The harvested cells were mixed with the media before centrifugation at a speed of 1000 rpm. For the experiments, 2×10^7 of the ICG-loaded macrophages were suspended in 1 ml of 10% (by weight) gelatin solution before being injected into phantoms and pig arterial tissues. The gelatin was used to simulate healthy tissue and to make the samples stable under the gravitational force acting on both the cells and the ICG particles during the experiments (Wang *et al* 2008).

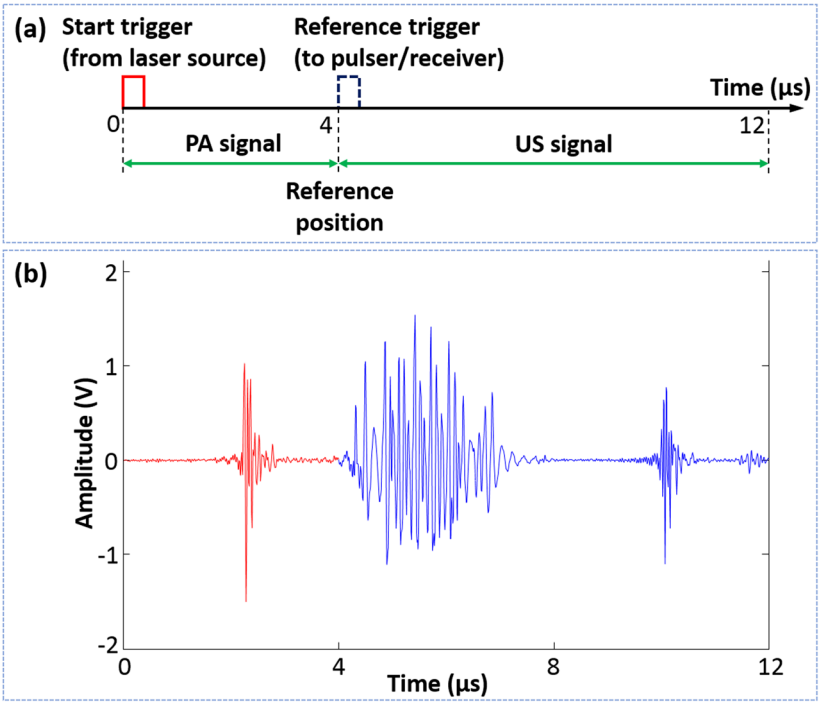

Figure 2. Demonstration of signal triggering and generation during IVUP imaging: (a) temporal sequence of synchronization for optical and ultrasonic signals and (b) PA and US signals achieved from a 80 μm human black hair with a single A-line scan. Note that the US signal includes both a triggering signal and an echo signal from the hair.

2.4. Sample preparation

Prior to tissue testing, blood vessel-mimicking phantoms with cells embedded were prepared to evaluate US and PA imaging under various conditions. The blood vessel-mimicking phantoms were constructed from a mixture of 8% polyvinyl alcohol (PVA; 363146 Aldrich, Sigma-Aldrich, MO, USA) and 0.4% fine ground silica (MIN-U-SIL®, U.S. SILICA, MD, USA). PVA was used as a base material for the vessel phantoms due to its non-toxic, easy casting, and long-term storage properties (Kharine *et al* 2003). The silica was used to mimic ultrasonic and optical scattering properties of biological tissue. The average diameter of the silica particles was 15 μm, which was comparable to the size of the cells of interest (about 21 μm in diameter for a human macrophage (Krombach *et al* 1997)). Figure 3(a) demonstrates a prepared phantom (30 mm long, 12 mm in outer diameter, and 1 mm wall thickness) consisting of four compartments. A 0.3 ml mixture of the ICG-loaded macrophages and 10% gelatin solution was injected into the top compartment whereas the bottom compartment was filled with a 0.3 ml mixture of ICG and 10% gelatin solution (concentration = 650 μM). For comparison purposes, only the 10% gelatin solution was added to the left compartment of the phantom. As a control, degassed water was injected into the middle lumen of the phantom as well as the right compartment (figure 3(a)). Prior to imaging experiments, a fabricated IVUP imaging catheter was inserted through the middle lumen of the phantom in order to remove any PA susceptibility artifacts. Then, the catheter was mechanically rotated inside the phantom to scan the entire lumen for the detection of the ICG-loaded macrophage cells.

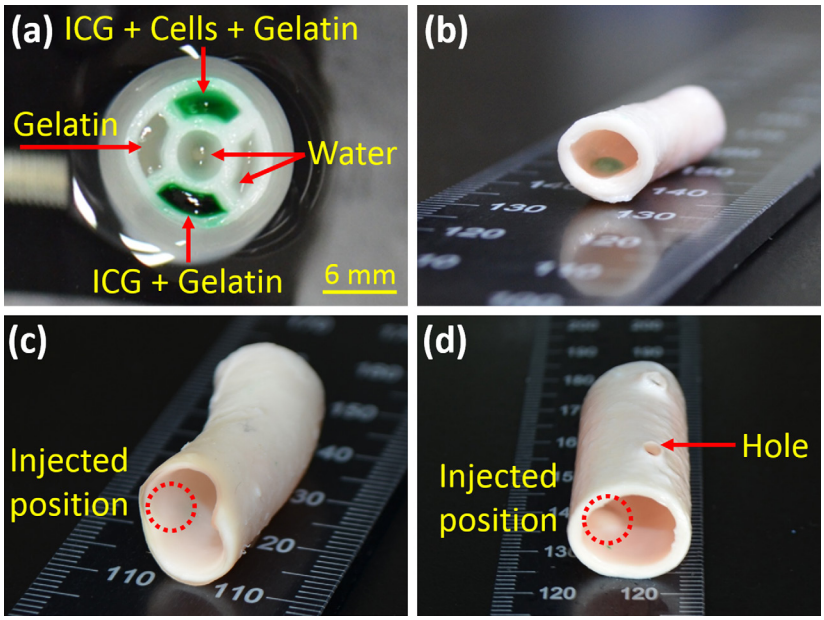

Figure 3. Phantom and *ex vivo* porcine tissue samples: (a) vessel-mimicking PVA phantom with four compartments (top: ICG-loaded macrophages; bottom: ICG solution in gelatin; left: gelatin, and right: water) and ICG-loaded macrophage-injected arterial tissues in diameters of (b) 8 mm, (c) 12 mm, and (d) 16 mm.

To evaluate the detectability and quantification of ICG-labeled macrophages by using the proposed IVUP imaging modality, *ex vivo* experiments were also performed on porcine arterial tissues with various outer diameters (8, 12, and 16 mm). The tissues were harvested from a local slaughter house and stored in saline at 4 °C to prevent dehydration prior to the experiments. Different volumes of the ICG-loaded macrophage cells mixed with 10% gelatin were injected with a syringe needle into the wall of the arterial samples in order to emulate various structures of atherosclerotic plaques in the blood vessel. Thus, 200, 50, and 100 μl of the ICG-loaded macrophages were applied to the arterial tissues in diameters of 8, 12, and 16 mm, respectively (figures 3(b)–(d)). A high volume (~200 μl) of ICG-loaded macrophages was injected into the 8 mm diameter artery to mimic a thick area of narrowing (~30% diameter stenosis) in the artery wall, which is frequently caused by high-risk atherosclerotic plaque. A very low volume (~50 μl) of ICG-loaded macrophages was injected into the 12 mm-diameter artery to emulate a thin layer of a fatty streak, which often grows with the inner layer of the artery wall in the early stages of atherosclerosis without any effect on blood flow. Lastly, a volume of 100 μl ICG-loaded macrophages was injected into the 16 mm-diameter artery. The injection volume was centrally located to create a thin area of narrowing (~9% diameter stenosis). The injection solution was distributed along a straight line and bulged out in the lumen of each arterial tissue. To validate the signal-to-noise ratio (SNR) at the far-field of the transducer imaging plane, a small hole (~4 mm in diameter) was created in the 16 mm tissue as a reference. After injection, each sample was placed in a water tank for the IVUP imaging. Similar to the phantom study, the IVUP imaging catheter was placed in the lumen of the arterial tissue and rotated using a stepper motor to perform the B-mode scans. A series of 20 B-mode scans with step sizes of 300, 250, and 450 μm was obtained from the three tissue samples

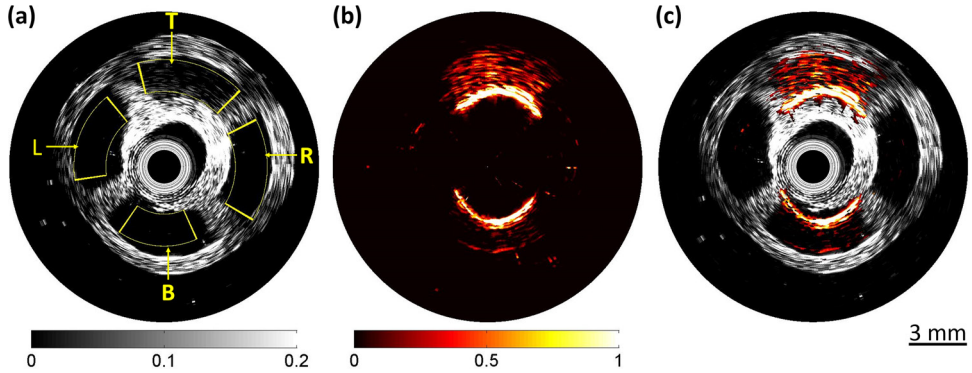

Figure 4. Cross-sectional images of vessel-mimicking phantoms with four compartments injected with ICG-loaded macrophages (top: *T*), ICG solution in gelatin (bottom: *B*), gelatin (left: *L*), and water (right: *R*). (a) IVUS image, (b) IVPA image at 800 nm, and (c) IVUP at 800 nm. The yellow boundaries in (a) represent the cut-off IVUS signals' length of 50 A-lines per each compartment for further averaging calculation.

(8, 12, and 16 mm diameters, respectively) along the axial direction of each sample in order to reconstruct 3D volumetric images. For statistical analysis, the Student's t-test was performed AQ8 and $p < 0.05$ denotes statistical significance.

3. Results

3.1. Phantom study

Figure 4 demonstrates cross-sectional images of vessel-mimicking phantoms with four compartments filled with ICG-loaded macrophages (*T*), ICG solution in water (*B*), gelatin (*L*), and water (*R*). Figures 4(a)–(c) represent the images acquired by IVUS, IVPA, and IVUP imaging, respectively, in a 16 mm diameter field of view (FOV). A series of rings in the center of both the IVUS and IVUP images marked the position of the fabricated IVUP catheter (figures 4(a) and (c)). To map signal intensity values, gray and hot color spaces were applied for the IVUS and IVPA images, respectively. The IVUS image in figure 4(a) demonstrates vividly the entire cross-sectional structure of the phantom with the four compartments. Although the cells loaded with ICG (*T*) were slightly visible due to acoustic scattering, the IVUS imaging was unable to display the presence of the ICG solution (*B*), gelatin (*L*), and water (*R*) on account of the lack of acoustic contrast. According to the IVPA image in figure 4(b), the IVPA technique was able to visualize the two compartments filled with ICG-loaded macrophages and ICG solution in water in light of the high image contrast. However, the other two were invisible due to the lack of optical absorption. Unlike IVUS, the IVPA imaging provided hardly any structural information about the phantom. On the other hand, the IVUP image in figure 4(c) clearly demonstrated both the position and the distribution of the inclusions in the sample. Both high ultrasonic and PA signal amplitudes represented the ICG-loaded macrophage cells (*T*), and only strong PA signals mirrored the response of the ICG solution (*B*). Due to the lack of acoustic interactions, neither the gelatin (*L*) or water (*R*) yielded any structural or functional information. The gap area between US and PA signals in compartment *B* of figure 4(c) was an uneven distribution of silica particles in the sample due to the handmade phantom.

In all of the experiments, 300 ultrasonic and PA beams were acquired for each B-mode scan. Per each compartment, only 50 A-lines were used to calculate and average IVUS signal

amplitudes to ensure that all the calculated signals were located inside the compartment. The signal lengths were also cut off (200 samples/total IVUP sampling length of 2000) to fit them inside the compartment areas (defined by the yellow boundaries in figure 4(a)). It was noted that the distance from the catheter to each compartment was different, so the boundaries differed along the circumference. Figure 5 presents a quantitative analysis of the PA and the US signal amplitudes measured from all the compartments, as shown in figure 4(c). Each signal was normalized using the maximum PA signal amplitude for comparison purposes. The top compartment was associated with the highest mean amplitudes of PA (1.00 ± 0.12) and US (0.21 ± 0.02; $p < 0.001$) signals. The PA imaging technique showed up to a 5-fold higher mean signal amplitude than the US imaging did ($p < 0.001$) in the top compartment. Compared to the pure ICG compartment (*B*), the top compartment entailed a 1.6 times high mean PA amplitude as that of the bottom compartment ($T = 1.00 \pm 0.12$ versus $B = 0.64 \pm 0.10$; $p < 0.001$). It was speculated that optical scattering inside the cells helped homogenize the incident light distribution over the volume of the top compartment. The compartments without cells or ICG (*L* and *R*) induced a relatively negligible generation of PA and US signals. It was noted that compartment *R* had a slightly higher US signal than both compartments *L* and *B* did (i.e. $R = 0.12 \pm 0.01$ versus $L = 0.09 \pm 0.01$, and $B = 0.1 \pm 0.01$) due to the random noise signals inside the boundary of compartment *R* (figure 4(a)).

3.2. Ex vivo study

IVUP imaging at a wavelength of 800 nm was performed on *ex vivo* porcine arterial tissue samples with ICG-loaded macrophages injected. Figures 6(a)–(c) shows IVUP images of the tissue with diameters of 8, 12, and 16 mm, respectively (FOV = 20 mm in diameter), which are displayed in gray and cool color maps. Overall, the IVUP images revealed both structural information about the arteries and also information about the spatial distribution of the ICG-loaded macrophages inside the arterial wall. Due to the largest injection volume (200 μl), figure 6(a) demonstrates the wide and deep distribution of the ICG-loaded cells across the tissue. The penetration depth reached ~3.5 mm in the 8 mm artery, which covered the entire tissue wall. Figure 6(b) presents the relatively faint color of the cell distribution in the 12 mm diameter tissue as the injection volume was 50 μl. In spite of having of the largest diameter (16 mm), the IVUP imaging was able to visualize the entire tissue structure along with the localized distribution of the ICG-loaded macrophages (100 μl) in the tissue wall (figure 6(c)). It was noted that a 4 mm hole as a reference was clearly identified in the acquired IVUP image in figure 6(c) due to a high SNR in the hole area (as discussed later).

Figure 7(a) presents the quantitative analysis on the total PA signals acquired from 30 A-lines in the injected positions of three atherosclerotic plaque-mimicking tissues in figure 6. The PA signals obtained from both the ICG-loaded macrophages and the background tissue were averaged, normalized, and displayed in cyan and gray colors, respectively. Overall, the mean PA signals measured from the macrophages were up to 10-fold higher than ones from the background ($p < 0.001$). The highest mean signal amplitude of the PA signals was detected at a region of interest from the 8 mm artery due to the largest injection volume of 200 μl (i.e. 1.00 ± 0.09 for 8 mm versus 0.78 ± 0.08 for 12 mm and 0.33 ± 0.03 for 16 mm; $p < 0.001$). In spite of a 50% smaller injection volume (50 μl for 12 mm versus 100 μl for 16 mm), the 12 mm artery still yielded a 2.4 times higher mean signal amplitude than the 16 mm artery (i.e. 0.78 ± 0.08 for 12 mm versus 0.33 ± 0.03 for 16 mm; $p < 0.001$). The higher mean signal detection could be associated with the shorter signal path length due to a 25% smaller diameter. Figure 7(b) demonstrates the spatial distribution of the PA signals

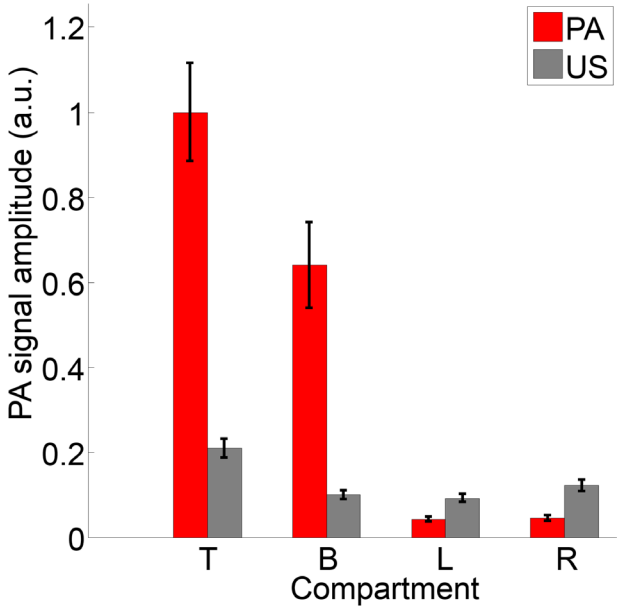

Figure 5. Quantitative analysis of normalized PA (in red) and US (in gray) signals acquired from four compartments injected with ICG-loaded macrophages (*T*), ICG solution in gelatin (*B*), gelatin (*L*), and water (*R*).

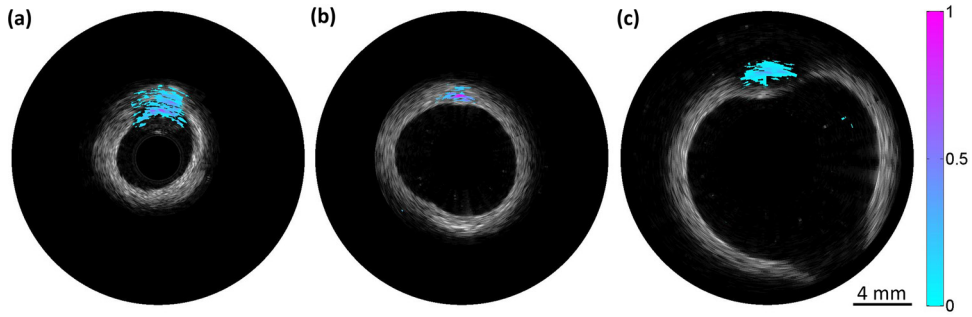

Figure 6. Cross-sectional IVUP images (at 800 nm) of atherosclerotic plaque-mimicking tissues in diameters of: (a) 8 mm, (b) 12 mm, and (c) 16 mm. Note that the colored areas represent the injection of ICG-loaded cells.

along the top side of the arterial tissue, as shown in the inlet (above dotted yellow line), as a function of the arc length. Similarly, the largest injection volume in the 8 mm artery resulted in a wider distribution of the ICG-loaded macrophages in the arterial tissue wall with higher signal amplitudes, in comparison with the other arterial tissues. The 12 mm artery yielded almost the same peak of the signal amplitude as the 8 mm artery but a narrower distribution due to the smaller amount of the ICG-loaded cell injection. Based upon the signal detection, most cells were primarily concentrated at the injection site. The 16 mm artery presented the lowest peak signal amplitude in the narrowest range. It was noted that the spatial distribution of the PA signals was rather dependent on both the injection volume and the artery diameter, but was independent of the volume of imaging targets. In fact, the smallest volume of the ICG-loaded cells implanted in the 12 mm artery offered a PA signal amplitude as high as that in the case

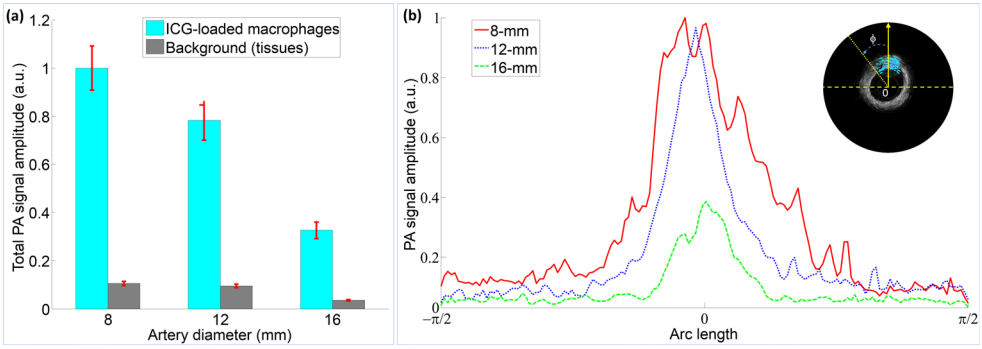

Figure 7. Quantitative analysis on PA signals from three arterial tissues (8, 12, and 16 mm in diameter): (a) normalized total signal amplitudes acquired from ICG labeled macrophages (cyan) and background tissue (gray) and (b) circumferential distribution of PA signal amplitudes from the top-half side of each tissue (above dotted line).

of the 8 mm artery with a 4-fold higher injection volume. However, the imaging target in the 12 mm artery was closer to the outer lining of the lumen wall, compared with that of the 8 mm one. Thus, both the target location and the distance could significantly affect the PA maximum amplitude signals in the artery.

Figures 8(a)–(c) show 3D volumetric IVUP images reconstructed from the samples with diameters of 8, 12, and 16 mm, respectively (FOV $= 20 \times 20\,\text{mm}^2$). Each image was displayed under the same viewpoint, as presented in the inlet in figure 8 (azimuthal angle $= 30°$ and elevation angle $= 60°$). US and PA signals were described in the gray and the cool color maps, respectively. In the homemade MATLAB program, transparency properties (alpha values) for the US imaging were set to be 20%, allowing the PA images to be visible. The alpha values of the PA imaging were modified to be 50%. The US images clearly depicted the entire shape and 3D structure of each tissue sample. Figure 8(c) confirms the reference hole in the middle of the tissue (16 mm diameter). Regardless of the artery diameter, all the reconstructed images displayed ICG-loaded macrophages injected inside the vessel walls under excitation at an 800 nm wavelength. Due to variations in signal amplitudes, the IVUP images vividly identified the distribution of the injected cells in the tissue. Figure 8(d) compares the normalized PA signal amplitudes along the sample (longitudinal direction and middle position) as a function of the B-mode scan number. It is evident that the 8 mm tissue shows highly concentrated cells at 2.4 mm away from the bottom of the tissue; this is due to the generation of the peak PA signal. Both the 12 mm and the 16 mm tissues exhibited relatively constant signal amplitudes (0.41 ± 0.04 for 12 mm and 0.11 ± 0.06 for 16 mm) along the arterial tissue, representing the even distribution of the cells in the tissue. The 12 mm was still associated with 4-fold higher signal amplitudes than the 16 mm ($p < 0.001$).

4. Discussion

The current study demonstrated the feasibility of detecting atherosclerotic plaques *ex vivo* with IVUP imaging by targeting macrophages labeled with ICG in porcine arterial tissues. Due to the strong light absorption of ICG at 800 nm, the combined imaging provided anatomical and molecular information about the plaque-mimicking arteries. The use of FDA-approved ICG has presented several clinically-excellent properties. Firstly, the IVUP imaging was able to monitor the ICG-labeled macrophages even at low concentrations (i.e. 1 mg ml^{-1} is

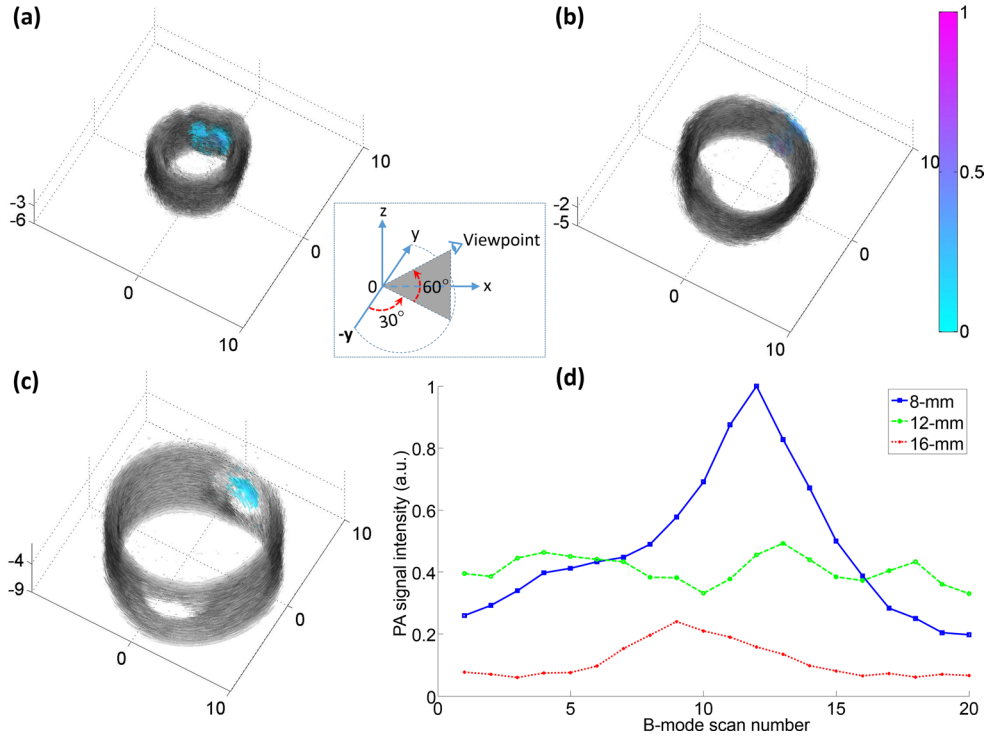

Figure 8. 3D volumetric IVUP images of atherosclerotic plaque-mimicking tissues with ICG-loaded macrophages injected in diameters of (a) 8 mm (200 μl injection), (b) 12 mm (50 μl injection), and (c) 16 mm (100 μl injection); (d) PA signal intensity acquired from injected cells along the vessel axis as a function of the B-mode scan number (up to 20 scans). The inset represents a viewpoint (30° of azimuth and 60° of elevation) for all the reconstructed images in the *xyz* coordinate.

non-toxic even after prolonged exposure (Kiilgaard *et al* 2006)) and low volumes (i.e. 50 μl). In particular, typical ICG concentrations used for *in vivo* retinal and choroidal angiography are 20–25 mg ml^{-1} (Ciamberlini *et al* 1997). Secondly, the nontoxic, nonionizing, and short lifetime in the blood circulation of ICG allow the repeated monitoring of the macrophages *in vivo*. Lastly, with the maximum optical absorption at 800 nm, ICG can prevent any light by AQ11 blood and water. In addition, the light scattering in biological tissues diminishes with increasing wavelengths and becomes minimal at the near-infrared region (i.e. 800 nm) (Jacques 2013). Therefore, ICG is the perfect contrast agent for deep imaging without tissue damage. Gold nanoparticles have also been applied to identify macrophages in atherosclerotic plaques (Wang *et al* 2008, 2010). However, light is strongly absorbed and scattered by blood at the peak absorption wavelength of gold nanoparticles, 532 nm, compared with the near-infrared regions. Furthermore, the most significant drawback of the nanoparticles was that the gold nanoparticles were not yet approved by the FDA for clinical applications.

Typically, the PA signal magnitude is linearly proportional to both the fluence of the incident laser light and the absorption coefficient of a sample (Yao and Wang 2014). In the *ex vivo* experiments, the optical absorption of the sample compositions is the same, while the laser fluences in the case of 12 and 16 mm arteries were lower than that from the 8 mm one due to the longer distance from the catheter to the imaging targets. However, the imaging targets' distribution in the 12 mm artery was closer to the outer lining of the lumen wall rather than

that of 8 and 16 mm ones; consequently, the PA magnitude signals in the case of the 12 mm artery was slightly decreased by the scattered light in biological tissues. In contrast, the imaging targets inside the 8 mm artery were behind a thick narrowing area. Thus, the PA magnitude signals were considerably affected by the scattered light in the tissues. The peak IVPA signal of the 12 mm vessel was highly comparable to that of the 8 mm vessel. On the other hand, both the long distance and the fact that it was behind a thin area of narrowing significantly affected the PA maximum amplitude signals in the case of the largest artery. According to *ex vivo* experiments, the 12 mm tissue with the 50 μl injection volume still yielded a 4-fold higher total PA signal amplitude than the 16 mm tissue with the 100 μl injection volume had. In spite of the 50% lower injection volume, the 12 mm sample had a 39% higher fluence than the 16 mm one did (i.e. 0.9 mJ cm^{-2} for 12 mm versus 0.55 mJ cm^{-2} for 16 mm) due to the relatively shorter distance between the sample and the transducer. It can be conceived that given the experimental conditions, the signal amplitude can be significantly contingent upon the number of delivered photons (i.e. laser fluence after absorbing and scattering by the medium/tissue) rather than the amount of ICG-loaded macrophage cells (i.e. optical absorption coefficient of the sample compositions). In fact, the 12 mm arterial tissue generated only a 22% lower total PA signal amplitude than the 8 mm one (i.e. 0.78 ± 0.08 for the 12 mm versus 1.00 ± 0.09 for the 8 mm) although the injection volume difference was 4-fold (i.e. 50 μl for the 12 mm versus 200 μl for the 8 mm).

Although macrophages are involved in many diseases related to the immune system, their pathophysiological roles in the diseases are still unclear. Thus, direct targeting of macrophages with minimally invasive IVUP imaging can help illuminate the functional diversity of macrophages and ultimately improve early detection, staging, and progression-tracking of disease-related macrophages. Visibility of PA imaging can be affected by not only the optical wavelength but also the imaging depth. Once the ICG-labeled macrophages were injected into arterial tissue, minimally invasive IVUP imaging could detect the existence of macrophages with relatively high spatial resolution and a penetration depth of several millimeters due to both unscattered and scattered light-inducing PA waves in biological tissues (Sethuraman *et al* 2007). Thus, such a penetration depth could be appropriate for the detection of vulnerable plaques (Sethuraman *et al* 2007). Besides, the system inherently has a limited lateral resolution that is dependent on the imaging depth; this is due to the use of an unfocused IVUS transducer element in the system. With the hole having a distance of around 8 mm from the transducer (figure 6(c)), the IVUS lateral resolving capability could be in the mm level. In this case, the hole was placed in the far field of the transducer. Although noise in the 4 mm hole area was observed in figure 6(c), it was readily recognized by the naked eye as the SNR of the tissue/hole areas was very high (SNR = 20 dB, as obtained by calculating the square of the root-mean-square amplitude ratio).

The key advantage of the proposed hybrid IVUP imaging is two-fold: (1) IVUP imaging can overcome the speckle artifacts of US by using light-induced ultrasonic waves, eventually achieving a high-contrast of optical images and (2) IVUP imaging can provide both the structure (by US) and composition (by PA) of the biological tissues simultaneously. Compared to CT and MRI, IVUP imaging is completely nonionizing in terms of radiation and it is also sensitive to soft tissues. In addition, IVUP imaging can be safer than PET for repeated monitoring at high resolutions and it can also provide deeper imaging on biological tissues without any degradation in the spatial resolution. The limitation of the current system is that it has a slow imaging speed due to the 10 Hz pulse repetition rate of the laser. For 300 ultrasonic and PA beams, a B-mode scan required a scanning time of 30 s. For a 3D volumetric imaging with a series of 20 B-mode scans, it takes over 10 min for a single wavelength irradiation light. However, the IVUP imaging system is based upon a high-speed imaging technique.

For example, in the case of the largest artery (16 mm in diameter) in this study, each A-line acquired 6000 samples, which equals the total record length of 30 μs (10 μs for PA and 20 μs for US signals) due to the 200 MS s^{-1} (200 samples μs^{-1}) DAQ card. The imaging depth, defined as the record length of the PA signal multiplied by the speed of sound in the working medium (i.e. ~1.5 mm μs^{-1} in water), was 15 mm. Such an imaging depth could be deep enough to visualize the structure of the largest human arteries. It can be assumed that the time delay between two consecutive laser and ultrasonic pulses is set to five times that of the total signal record length (i.e. 5×30 μs $= 150$ μs). Then, the data acquisition time of the current imaging system for a single A-line is merely 180 μs. As a result, the repetition rate of the laser can be as high as 1/(180 μs) $\approx$ 5.5 kHz and, then, the time for a series of 20 B-mode scans, including 300 A-line per each scan, could be $20 \times 300 \times 180$ μs $= 1.1$ s. A high-speed (~1.0 s per frame) IVPA imaging of atherosclerotic plaque has recently been reported using a 2 kHz laser (Wang *et al* 2014). Another limitation in the current system was the repetition rate of the continuous reverse rotation of the motor as high-speed scanning was alternated in clockwise and counterclockwise directions. With almost no load condition (the catheter weight ~0.6 g), a normal stepper motor can achieve a repetition rate of 20 scans per 1.1 s. However, with a higher repetition rate, the use of a voice coil motor may be necessary to maintain the stability and durability of the motor.

Normally, delay generators are used to provide a single scan containing both PA and US signals in all the published systems (Sethuraman *et al* 2007, Wang *et al* 2010, Karpiouk *et al* 2012, Yang *et al* 2012, Bai *et al* 2014). Unlike the previous methods, we could perform the same function without using any external device. Not using additional equipment such as delay generators (Sethuraman *et al* 2007, Wang *et al* 2010, Karpiouk *et al* 2012, Yang *et al* 2012, Bai *et al* 2014), micro-motors and scanning mirror, as in Yang *et al* (2012), or an optical rotary joined with electrical slip rings, as in Bai *et al* (2014), can save significant costs, while the system can fully implement the same functionality (i.e. 3D scanning and single scan combining US and PA signals), compared with published systems. With the high-frequency transducer, the US and PA signals were resolved with a spatial resolution in the order of the microscopic level (Sethuraman *et al* 2007), and such a resolution could be desirable for the detection of vulnerable plaques (Wang *et al* 2010).

In all of the experiments, the applied optical power was set at 0.42 mW, and the corresponding pulse energy was 0.042 mJ at 10 Hz. With a polished angle of 38 degrees and a fiber diameter of 0.6 mm, the area of the output end surface of the MOF was estimated to be 0.46 mm^2. In water, the fiber had the maximum acceptance angle of 9.5 degrees as NA $= 0.22$. Therefore, the incident laser intensity on the sample surface was maintained lower than 9.1 mJ cm^{-2} (i.e. ~29% of the safety limit) during the entire experiment. Hence, the laser fluence used in our experiments satisfied the ANSI safety limit (i.e. $20 \times 100.002(\lambda - 700) \approx$ 31.7 mJ cm^{-2}) for skin surface exposure at a selected wavelength.

5. Conclusion

The current study demonstrated the feasibility of IVUP imaging to provide spatial and functional information on the light distribution in phantoms and tissues for potentially identifying atherosclerotic plaques. The proposed hybrid imaging with delayed signal sequences was able to visualize the entire tissue structure as well as detect the distribution of the ICG-loaded macrophages in the tissue. Due to the strong light absorption of ICG at 800 nm, the IVUP imaging yielded strong PA responses from the localized cells in the tissue, leading to high imaging contrast and sensitivity. Further studies will be conducted on atherosclerotic diseased

rabbit aorta *in vivo* to demonstrate the imaging capability for detecting high-risk plaques in arterial tissue. The proposed IVUP technique could be a feasible imaging modality to identify atherosclerotic plaques in an endoscopic manner.

AQ12 ## Acknowledgments

AQ13

This research was supported by a grant from the Marine Biotechnology Program (20150220) funded by the Ministry of Oceans and Fisheries, Republic of Korea.

AQ14 ## References

Bai X, Gong X, Hau W, Lin R, Zheng J, Liu C, Zeng C, Zou X, Zheng H and Song L 2014 Intravascular optical-resolution photoacoustic tomography with a 1.1 mm diameter catheter *PLoS One* **9** e92463

Benson R C and Kues H A 1978 Fluorescence properties of indocyanine green as related to angiography *Phys. Med. Biol.* **23** 159

Bui N Q, Hlaing K K, Nguyen V P, Nguyen T H, Oh Y-O, Fan X F, Lee Y W, Nam S Y, Kang H W and Oh J 2015 Intravascular ultrasonic–photoacoustic (IVUP) endoscope with 2.2 mm diameter catheter for medical imaging *Comput. Med. Imaging Graph.* **45** 57–62

Caesar J, Shaldon S, Chiandussi L E, Guevara L and Sherlock S 1961 The use of indocyanine green in the measurement of hepatic blood flow and as a test of hepatic function *Clin. Sci.* **21** 43

Ciamberlini C, Guarnieri V, Longobardi G, Poggi P, Donati M and Panzardi G 1997 Indocyanine green videoangiography using cooled charge-coupled devices in central serous choroidopathy *J. Biomed. Opt.* **2** 218–25

De Montigny E 2011 Photoacoustic tomography: principles and applications Department of Physics
AQ15 Engineering, Polytechnic School Montreal

Desmettre T, Devoisselle J and Mordon S 2000 Fluorescence properties and metabolic features of indocyanine green (ICG) as related to angiography *Surv. Ophthalmol.* **45** 15–27

Fischer T, Gemeinhardt I, Wagner S, Stieglitz D V, Schnorr J, Hermann K-G A, Ebert B, Petzelt D, MacDonald R and Licha K 2006 Assessment of unspecific near-infrared dyes in laser-induced fluorescence imaging of experimental arthritis *Acad. Radiol.* **13** 4–13

Flower R W 1995 Evolution of indocyanine green dye choroidal angiography *Opt. Eng.* **34** 727–36

Fox I, Brooker L, Heseltine D, Essex H and Wood E 1957 *Proc. of the Staff Meetings (Mayo Clinic,*
AQ16 *1957)* vol 32 p 478

Hwang B-H, Kim M-H and Chang K 2011 Molecular imaging of high-risk atherosclerotic plaques: is it clinically translatable? *Korean Circ. J.* **41** 497–502 AQ17

Jacques S L 2013 Optical properties of biological tissues: a review *Phys. Med. Biol.* **58** R37

Jansen K, Wu M, van der Steen A F and van Soest G 2013 Lipid detection in atherosclerotic human coronaries by spectroscopic intravascular photoacoustic imaging *Opt. Express* **21** 21472–84

Karpiouk A B, Wang B, Amirian J, Smalling R W and Emelianov S Y 2012 Feasibility of *in vivo* intravascular photoacoustic imaging using integrated ultrasound and photoacoustic imaging catheter *J. Biomed. Opt.* **17** 0960081–6

Kharine A, Manohar S, Seeton R, Kolkman R G, Bolt R A, Steenbergen W and de Mul F F 2003 Poly (vinyl alcohol) gels for use as tissue phantoms in photoacoustic mammography *Phys. Med. Biol.* **48** 357

Kiilgaard J F, Nissen M H and La Cour M 2006 An isotonic preparation of 1 mg ml^{-1} indocyanine green is not toxic to hyperconfluent ARPE19 cells, even after prolonged exposure *Acta Ophthalmol. Scand.* **84** 42–6

Krombach F, Münzing S, Allmeling A-M, Gerlach J T, Behr J and Dörger M 1997 Cell size of alveolar macrophages: an interspecies comparison *Environ. Health Perspect.* **105** 1261

Libby P, Ridker P M and Hansson G K 2009 Inflammation in atherosclerosis: from pathophysiology to practice *J. Am. Coll. Cardiol.* **54** 2129–38

Rudd J H, Warburton E, Fryer T, Jones H, Clark J, Antoun N, Johnström P, Davenport A, Kirkpatrick P and Arch B N 2002 Imaging atherosclerotic plaque inflammation with [18F]-fluorodeoxyglucose positron emission tomography *Circulation* **105** 2708–11

Schmitz S A, Taupitz M, Wagner S, Wolf K J, Beyersdorff D and Hamm B 2001 Magnetic resonance imaging of atherosclerotic plaques using superparamagnetic iron oxide particles *J. Magn. Reson. Imaging* **14** 355–61

Sethuraman S, Aglyamov S R, Amirian J H, Smalling R W and Emelianov S Y 2007 Intravascular photoacoustic imaging using an IVUS imaging catheter *IEEE Trans. Ultrason. Ferroelectr. Freq. Control* **54** 978–86

Stanga P E, Lim J I and Hamilton P 2003 Indocyanine green angiography in chorioretinal diseases: indications and interpretation: an evidence-based update *Ophthalmology* **110** 15–21

Tahara N, Kai H, Ishibashi M, Nakaura H, Kaida H, Baba K, Hayabuchi N and Imaizumi T 2006 Simvastatin attenuates plaque inflammation: evaluation by fluorodeoxyglucose positron emission tomography *J. Am. Coll. Cardiol.* **48** 1825–31

Tang T Y, Howarth S P, Miller S R, Graves M J, Patterson A J, Jean-Marie U, Li Z Y, Walsh S R, Brown A P and Kirkpatrick P J 2009 The ATHEROMA (atorvastatin therapy: effects on reduction of macrophage activity) study: evaluation using ultrasmall superparamagnetic iron oxide-enhanced magnetic resonance imaging in carotid disease *J. Am. Coll. Cardiol.* **53** 2039–50

Tawakol A, Migrino R Q, Bashian G G, Bedri S, Vermylen D, Cury R C, Yates D, LaMuraglia G M, Furie K and Houser S 2006 *In vivo* 18F-fluorodeoxyglucose positron emission tomography imaging provides a noninvasive measure of carotid plaque inflammation in patients *J. Am. Coll. Cardiol.* **48** 1818–24

Trivedi R A, Mallawarachi C, Jean-Marie U, Graves M J, Horsley J, Goddard M J, Brown A, Wang L, Kirkpatrick P J and Brown J 2006 Identifying inflamed carotid plaques using *in vivo* USPIO-enhanced MR imaging to label plaque macrophages *Atertioscler. Thromb. Vasc. Biol.* **26** 1601–6

Van Gils J M, Derby M C, Fernandes L R, Ramkhelawon B, Ray T D, Rayner K J, Parathath S, Distel E, Feig J L and Alvarez-Leite J I 2012 The neuroimmune guidance cue netrin-1 promotes atherosclerosis by inhibiting the emigration of macrophages from plaques *Nat. Immunol.* **13** 136–43

Vinegoni C, Botnaru I, Aikawa E, Calfon M A, Iwamoto Y, Folco E J, Ntziachristos V, Weissleder R, Libby P and Jaffer F A 2011 Indocyanine green enables near-infrared fluorescence imaging of lipid-rich, inflamed atherosclerotic plaques *Sci. Transl. Med.* **3** 84ra45

Vo-Dinh T, Oraevsky A A and Karabutov A A 2003 *Biomedical Photonics Handbook* (Boca Raton, FL: CRC Press)

Waldeck J, Häger F, Höltke C, Lanckohr C, von Wallbrunn A, Torsello G, Heindel W, Theilmeier G, Schäfers M and Bremer C 2008 Fluorescence reflectance imaging of macrophage-rich atherosclerotic plaques using an $\alpha v\beta 3$ integrin–targeted fluorochrome *J. Nucl. Med.* **49** 1845–51

Wang B, Su J L, Karpiouk A B, Sokolov K V, Smalling R W and Emelianov S Y 2010 Intravascular photoacoustic imaging *IEEE J. Sel. Top. Quantum Electron.* **16** 588–99

Wang B, Yantsen E, Larson T, Karpiouk A B, Sethuraman S, Su J L, Sokolov K and Emelianov S Y 2008 Plasmonic intravascular photoacoustic imaging for detection of macrophages in atherosclerotic plaques *Nano Lett.* **9** 2212–7

Wang L V 2009 *Photoacoustic Imaging and Spectroscopy* (Boca Raton, FL: CRC Press)

Wang P, Ma T, Slipchenko M N, Liang S, Hui J, Shung K K, Roy S, Sturek M, Zhou Q and Chen Z 2014 High-speed intravascular photoacoustic imaging of lipid-laden atherosclerotic plaque enabled by a AQ18 2 kHz barium nitrite raman laser *Sci. Rep.* **4**

Yang J-M, Chen R, Favazza C, Yao J, Li C, Hu Z, Zhou Q, Shung K K and Wang L V 2012 A 2.5 mm diameter probe for photoacoustic and ultrasonic endoscopy *Opt. Express* **20** 23944–53

Yao J and Wang L V 2014 Sensitivity of photoacoustic microscopy *Photoacoustics* **2** 87–101

Yoneya S, Saito T, Komatsu Y, Koyama I, Takahashi K and Duvoll-Young J 1998 Binding properties of indocyanine green in human blood *Invest. Ophthalmol. Vis. Sci.* **39** 1286–90

Yoo J S, Das R K, Jow Z Y and Chang Y-T 2014 *In vivo* detection of macrophage recruitment in hind-limb ischemia using a targeted near-infrared fluorophore *PLoS One* **9** e103721